

Article

# Coupling the Microscopic Healing Behaviour of Coatings to the Thermoreversible Diels-Alder Network Formation

Joost Brancart <sup>1,2,\*</sup> , Robrecht Verhelle <sup>1</sup>, Jessica Mangialetto <sup>1</sup> and Guy Van Assche <sup>1</sup>

<sup>1</sup> Department of Materials and Chemistry, Physical Chemistry and Polymer Science, Vrije Universiteit Brussel, Pleinlaan 2, B-1050 Brussels, Belgium; robrecht.verhelle@vub.be (R.V.); jessica.mangialetto@vub.be (J.M.); guy.van.assche@vub.be (G.V.A.)

<sup>2</sup> Department of Mechanical Engineering, Robotics and Multibody Mechanics, Vrije Universiteit Brussel, Pleinlaan 2, B-1050 Brussels, Belgium

\* Correspondence: joost.brancart@vub.be; Tel.: +32-2-629-32-89

Received: 25 November 2018; Accepted: 22 December 2018; Published: 26 December 2018



**Abstract:** While thermally reversible polymer network coatings based on the Diels-Alder reaction are widely studied, the mechanisms responsible for the heating-mediated healing of damage is still not well understood. The combination of microscopic evaluation techniques and fundamental insights for the thermoreversible network formation in the bulk and coating shed light on the mechanisms behind the damage healing events. The thermomechanical properties of thermoset and elastomer coatings, crosslinked by the furan-maleimide Diels-Alder cycloaddition reaction, were studied in bulk and compared to the thermal behaviour applied as coatings onto aluminium substrates. The damage sealing of thermoset ( $T_g = 79$  °C) and elastomer ( $T_g = -49$  °C) coatings were studied using nano-lithography and atomic force microscopy (AFM). The sealing event is studied and modelled at multiple temperatures and correlated to the changes in the network structure and corresponding thermomechanical properties.

**Keywords:** Diels-Alder; reversible polymer network; dynamic covalent; self-healing; modelling

## 1. Introduction

Since their introduction in polymer science, many self-healing mechanisms have been incorporated into coatings and surfaces [1]. Extrinsic healing systems—commonly referred to as autonomous healing systems—rely on the encapsulation of a healing agent in containers such as microcapsules [2–4]. Their main drawback for thin layer applications is the localized and discrete distribution of the healing agent inside the polymer matrix and the layer thickness restriction resulting from the size of the containers. These drawbacks can be reduced by reducing the size of the containers, while the distribution of the healing agent and the locally available amounts can be further improved by the use of nanovascular systems [5,6]. Intrinsic healing mechanisms, which are inherent to the polymer matrix chemistry, do not pose these drawbacks, and many chemistries have been proposed for coatings and thin layer applications. In general, physicochemical interactions (e.g., hydrogen bonding [7,8]) are distinguished from reversible covalent chemistries (e.g., reversible (cyclo)addition reactions [9–14]). Physicochemical interactions are much weaker than reversible covalent bonds. Therefore, they are usually broken and (re)formed much faster.

Recently, so-called multiple-action self-healing coatings have been developed, exhibiting multiple mechanisms that provide enhanced and prolonged corrosion protection of the coated materials. A self-healing mechanism of the coating is combined with a corrosion inhibitor that is distributed

or encapsulated in the coating matrix and subsequently released upon damage [15,16]. In addition, multi-layer coatings are proposed where different layers provide different functions [17]. In other cases, corrosion inhibition properties are attributed to the chemistry of the polymer matrix, e.g., aniline trimers [18]. In the latter case, the polymer matrix exhibits both the anticorrosion and self-healing properties.

Healing of damage in reversible polymer network systems can be divided in two types of mechanisms. Either the damage is healed under the application conditions, or an external stimulus is applied to activate the healing action. For the thermally reversible polymer networks based on the furan and maleimide Diels-Alder chemistry, room-temperature healing was compared to heating-mediated healing in a previous work [19]. In case of heating-mediated healing, two steps can be distinguished: First, the damage is sealed at elevated temperatures, and next, the mechanical properties are recovered at lower temperatures by a re-establishing of the (thermoreversible) links. When healing at room temperature, the healing action involves the reformation of the (reversible) covalent bonds that were previously broken during mechanical activation. Healing of macroscopic damage is only possible if enough mobility is present for the polymer chains to find reactive partners across the damage surfaces. In general, depending on the size and geometry of the damage, more mobility may be required. As scratches in coatings may be wider than the thickness of the coating, a high degree of mobility may be required to seal the damage area. In this paper, the heating-mediated healing of scratches in thin coatings is studied. The scope of this paper is limited to studying the damage sealing event using microscopic techniques.

In earlier work, the use of atomic force microscopy was proposed as a valuable tool for the healing investigation of microscopic damage [20]. Local thermal analysis allows the determination of thermomechanical behaviour at the microscopic scale, whereas nano-indentation is used to create well-controlled microscopic damage. Similarly, other studies have reported the advantage of a localized evaluation of the healing performance [21,22] and corrosion protection [23,24] of coatings. In this work, polymer networks that are reversibly crosslinked by the Diels-Alder cycloaddition reaction are considered. They have attracted much interest in coating science research due to their ability to restore the barrier properties after damage [20,25]. The reversibility of the Diels-Alder reaction and its effect on the reversible network formation are well established in literature [25,26]. Detailed knowledge of the healing mechanism and of structure-property relationships allows tuning of the thermomechanical properties and thermal responsiveness [26] and of the healing behaviour [19]. In this work, the thermomechanical behaviour and thermochemistry of dynamically reversible polymer networks are linked to the coating properties and the microscopic healing behaviour of thin layers upon damage and to related limitations.

## 2. Materials and Methods

### 2.1. Materials

Furfuryl glycidyl ether (FGE, 96%) and 1,1'-(Methylenedi-4,1-phenylene) bismaleimide (DPBM, 95%) were purchased from Sigma-Aldrich (Overijse, Belgium). The Jeffamine D series amine hardeners were kindly supplied by Huntsman Corporation (Everberg, Belgium). Jeffamines D230 ( $M_n = 257 \text{ g} \cdot \text{mol}^{-1}$ ), D400 ( $M_n = 471 \text{ g} \cdot \text{mol}^{-1}$ ), D2000 ( $M_n = 2575 \text{ g} \cdot \text{mol}^{-1}$ ), and D4000 ( $M_n = 4415 \text{ g} \cdot \text{mol}^{-1}$ ) were furan-functionalized using the synthesis method described in an earlier work [25]. The degree of functionalization was about 95%, resulting in a furan functionality of 3.8 for the functionalized Jeffamines. Figure 1 shows the chemical structures of the building blocks of the reversible networks.

The crystalline bismaleimide DPBM was dissolved into chloroform with stoichiometric amounts of the furan-functionalized amines F230, F400, F2000, or F4000 and mixed until a clear, homogeneous solution is obtained (10–20 wt.%). The solution was then spin coated onto 0.5 mm thick pure aluminium (Al1050, 15 mm × 15 mm) substrates using a SPIN150-v3 spin coater from SPS-Europe (Brecht, Belgium). Spin coating at a rotation speed of 2000 rpm and an acceleration of  $1000 \text{ rpm} \cdot \text{s}^{-1}$  for 60 s

produces coatings of the order of 1  $\mu\text{m}$  thickness. This thickness is ideal for local thermal analysis measurements, as the penetration of the tip into the material can only be a small fraction of the size of the tip itself. Bulk samples were prepared by casting the monomer solution in Teflon moulds and subsequent solvent removal above their gel transition temperatures, under vacuum. The coatings and bulk samples were cured at 30  $^{\circ}\text{C}$  for at least 3 days to form the Diels-Alder crosslinks.

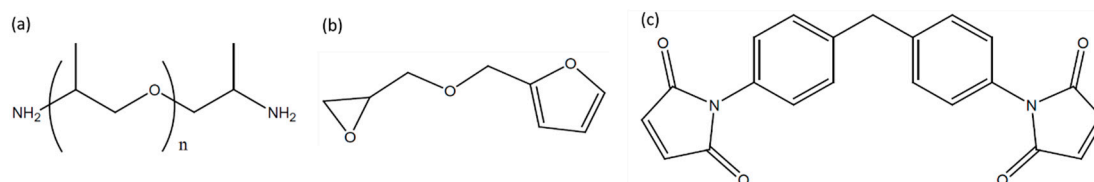


**Figure 1.** Components of the reversible network coatings: (a) Jeffamine D series amine hardeners; (b) furfuryl glycidyl ether (FGE); and (c) 1,1'-(Methylenedi-4,1-phenylene) bismaleimide (DPBM).

## 2.2. Instruments

### 2.2.1. Dynamic Rheology

Dynamic rheology measurements were performed on an AR-G2 rheometer from TA Instruments (Asse, Belgium), equipped with electrically heated plates to study the rheological behaviour as a function of temperature. The measuring geometry was shielded from the outside by a heat shield to maximize the temperature control and to minimize the temperature gradient across the studied sample. All rheometry experiments were performed using 15 mm disposable aluminium parallel plates. The rheometer and geometry were calibrated prior to every experiment. Step-wise isothermal small-angle oscillatory shear measurements were performed at discrete frequencies. The amplitude was adjusted from 1% in the predominantly elastic state to 10% in the viscous state. The step time at every temperature was optimized to ensure thermal and chemical equilibrium.

### 2.2.2. Dynamic Mechanical Analysis

A TA Instruments Q800 Dynamic Mechanical Analyzer (DMA, TA Instruments) was equipped with a gas cooling accessory (GCA) unit, allowing cooling to temperatures below  $-150$   $^{\circ}\text{C}$ . All specimens were tested in tensile testing mode using the Tension/Film clamp set-up by TA Instruments. The clamp was calibrated daily. Small-amplitude dynamic mechanical measurements were performed in a heating at 1  $\text{K}\cdot\text{min}^{-1}$  to have negligible temperature gradients within the tested specimen.

### 2.2.3. Atomic Force Microscopy

Topography measurements were performed using an Asylum Research MFP3D™ Atomic Force Microscope (AFM, Oxford Instruments, High Wycombe, UK) equipped with an Olympus AC160TS-E2 AFM tip for topography imaging in tapping mode. The AFM was equipped with the Asylum research PolyHeater for controlled heating of the studied sample.

Nanolithography was used to create defects of different types, sizes, and geometries using a well-defined force along a programmed path. The AFM tips were calibrated for reproducible force application on the coating surface (typical resonance frequency of around 350 MHz and spring constant of 20 to 30  $\text{N}\cdot\text{m}^{-1}$ ). The force was ramped along the programmed path from 0 to 10 V ( $\sim 15$   $\mu\text{N}$ ). Prior to self-healing assessment, the coatings were allowed to recover elastic deformation to separate the healing event from any elastic recovery.

In general, the volume of the scratch is the best parameter to characterize the remaining damage, taking into account geometric variations of the damage volume. In this work, the magnitude of the damage was characterized by the depth of the scratch, since it is more easily determined from the topography images, and since it is (roughly) proportional to the damage volume, as the width of damage at the surface remains roughly constant.

Local thermal analysis (LTA) measurements were performed using a TopoMetrix Explorer AFM (TopoMetrix Corporation, Santa Clara, CA, USA) equipped with a Veeco 1610-00 Wollaston thermal resistor (Veeco, Aschheim/Dornach Munich, Germany) AFM tip (5  $\mu\text{m}$  Pt/Rh filament) as the sample and reference probe. Temperature calibration was performed using the surface melting of a PET film and the set point temperature (30  $^{\circ}\text{C}$ ) of the TA Instruments heat/cool stage on which the sample was mounted. The sensor versus temperature plot gives the vertical position of the probe tip as it is heated. The sensor signals are corrected for thermal expansion of the coating material and the underlying substrate material by means of a baseline tilt.

### 3. Results

#### 3.1. Dynamic Reversibility of Diels-Alder Cycloadducts

The dynamic character of the Diels-Alder cycloaddition reaction between furan and maleimide groups has been thoroughly evaluated in previous work [26]. The reversibility of the network formation (gelation) was studied in great detail. In recent work the effect of the stereochemistry on this reversible network formation was further elaborated and the implications on possible applications were discussed [27]. With respect to self-healing coating applications, the effect of the stereochemistry of the Diels-Alder reaction on the properties of the thermoreversible coating does not need to be considered, as the mechanical force exerted on the coating surfaces is sufficiently large not to discriminate between the bond strengths of both stereoisomer adducts. For the thermal response and kinetic simulations, the formation of both endo and exo adduct is taken into account. However, as this does not impact the discussion and conclusions, the stereochemistry will not be further considered in this paper.

Using the kinetic parameters for the reaction between the furan-functionalized Jeffamines and the aromatic bismaleimide DPBM (Table A1 in Appendix A), the equilibrium conversion of the reversible Diels-Alder reaction can be calculated as a function of temperature for a fixed concentration of furan and maleimide functional groups (Figure 2a) or as a function of concentration at a fixed reference temperature (Figure 2b), using Equation (1), where  $[M]_0$  is the initial concentration of maleimide groups in the polymer network coating.

$$x_{\text{eq}} = \frac{K[M]_0 - \sqrt{(K[M]_0)^2 - 4K^2[M]_0^2}}{2K[M]_0} \quad (1)$$

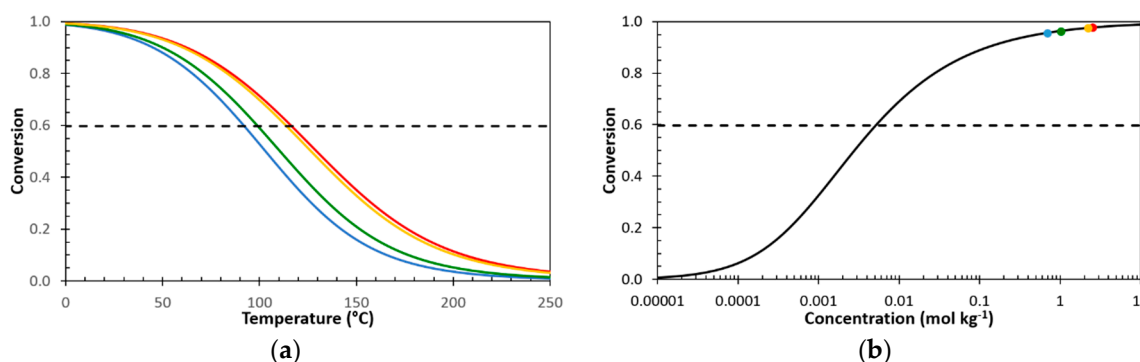


**Figure 2.** Diels-Alder conversion for stoichiometric FGE-DPBM-based systems as a function of temperature (a) and as a function concentration at a reference temperature of 25  $^{\circ}\text{C}$  (b). The concentrations and corresponding conversions for the different thermoreversible polymer networks are indicated: DPBM-F230 (red), -F400 (yellow), -F2000 (green), and -F4000 (blue). The gel conversion for a 4 + 2 network system is indicated (dashed horizontal line).

The reaction rate constants  $k$  can be calculated at a temperature  $T$  using the kinetic parameters in Table A1 and Equation (A1) in Appendix A. From these rate constants  $k$  the equilibrium constant  $K$  can be derived using Equation (A2). Upon heating, the Diels-Alder conversion decreases with increasing temperature, as the retro Diels-Alder reaction becomes relatively more important and the equilibrium is gradually shifting towards the monomers. At a certain temperature and time the conversion will drop below the critical gel conversion  $x_{gel}$ , indicated by the horizontal dashed line in Figure 2. For the combination of the furan-functionalized Jeffamines ( $f_F = 3.8$ ) with a bismaleimide ( $f_M = 2$ ) the theoretical  $x_{gel}$  equals 0.60. Below this critical conversion the material is no longer a network. The equilibrium gel point temperature  $T_{gel,eq}$  can be determined as the temperature at which the equilibrium conversion  $x_{eq}$  equals the critical gel conversion  $x_{gel}$ . When kept above this temperature, the material loses its mechanical stability and shows viscous flow behaviour. For each reversible network,  $x_{eq}$  depends on the concentration of the active groups and, consequently, so does  $T_{gel,eq}$ . The  $T_{gel,eq}$  for the different networks studied in this work are listed in Table 1. Similarly, the conversion and gel point can be determined in off-equilibrium conditions, using a predefined temperature profile (see Section 3.1.1).

**Table 1.** Thermophysical properties of the reversible polymer network systems.

Network	$[M]_0$ (mol kg <sup>-1</sup> )	$T_g$ (°C) <sup>1</sup>	$E'$ (MPa) <sup>2</sup>	$T_{gel,eq}$ (°C)	$T_{gel}$ (°C) <sup>3</sup>	$T_{soft}$ (°C)
DPBM-F230	2.52	95	$>2 \times 10^3$	116	130	118
DPBM-F400	2.22	79	$2.3 \times 10^3$	114	120	114
DPBM-F2000	1.02	-47	65	99	97	104
DPBM-F4000	0.69	-60	6.4	92	91	85

<sup>1</sup>: Maximum of the loss modulus  $E''$  in DMA at 1 Hz; <sup>2</sup>: DMA in tension at 30 °C, 1 Hz and 0.1% strain; <sup>3</sup>: Determined as the frequency-independent cross-over of the loss angle in dynamic rheometry.

It should thus be highlighted that the equilibrium Diels-Alder conversion also depends on the initial concentration of the furan and maleimide groups, as illustrated in Figure 2b at 25 °C. The equilibrium conversions represent the final conversion after the equilibrium is installed between furan, maleimide and the formed cycloadducts at the initial concentrations of furan and maleimide. In this figure, the equilibrium conversions for the network systems used in this work are indicated at their respective initial maleimide and furan concentrations. These results are valid for stoichiometric mixtures of furan and maleimide groups. A similar approach can be used for off-stoichiometric mixtures, in which case both the equilibrium curve and the gel conversion will change. The decrease in the equilibrium Diels-Alder conversion  $x_{eq}$  with decreasing initial concentration (Figure 2b) implies that the conversion drops below the critical gel conversion  $x_{gel}$ , indicated by the horizontal dashed line. As stated earlier, below this critical conversion the material is no longer a network, which implies that using a good solvent the polymer network can be (reversibly) dissociated and dissolved. As the solvent swells the reversible polymer network, the concentration of the reactive groups decreases. Following Le Chatelier's principle, the decrease in concentration will result in a shift of the Diels-Alder equilibrium from the cycloadducts towards the furan and maleimide reactants. As the cross-link density of the network decreases due to the breaking of cycloadduct bonds, the network can be further swollen, diluting the reactive system, and decreasing the equilibrium conversion to the point where the conversion drops below the gel conversion and the network is no longer present. The broken-down network continues to dissociate and dissolve until the equilibrium condition is reached. It should be noted that this is only possible using a good solvent for the polymer network chemistry, as the solvent needs to be able to diffuse into the polymer network to swell it. For use as coatings in contact with highly concentrated solvent, the chemistry of the polymer matrix should be adapted to avoid compatibility. For outdoor applications, a polymer matrix that does not allow water infiltration is advisable, both to ensure the stability of the coating and to prevent corrosion due to diffusion of water to an underlying metal substrate.

### 3.1.1. Thermomechanical Behaviour

Using dynamic rheometry, the gel transition temperature can be determined as the temperature at which the loss angle  $\delta$  becomes frequency independent [28]. The dynamic rheometry experiments in Figure 3a show how the (reversible) gel transition temperature increases with increasing initial concentrations of the furan and maleimide functional groups in the respective polymer networks. These values are tabulated in Table 1 and compare favourably to the theoretical values for the equilibrium gel transition temperature  $T_{gel,eq}$  that were determined earlier as the temperature at which the equilibrium conversion  $x_{eq}$  equals the gel conversion  $x_{gel}$  of 0.58 for a 4 + 2 reactive system.

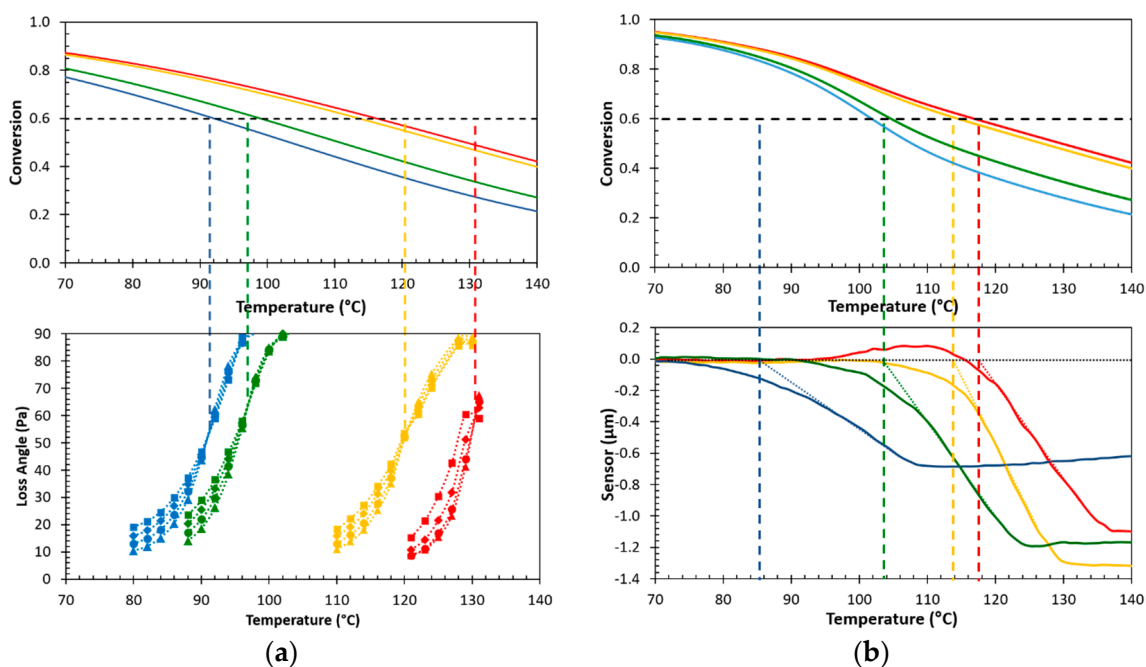


**Figure 3.** (a) Dynamic rheology measurements related to the equilibrium conversion simulations and (b) local thermal analysis measurements with the corresponding conversion profiles during heating of the LTA probe at  $0.6 \text{ K}\cdot\text{min}^{-1}$  for DPBM-F230 (red), -F400 (yellow), -F2000 (green), and -F4000 (blue).

Figure 3b shows the local thermal analysis (LTA) results of the same polymer networks applied as coatings onto aluminium substrates. As the tip of the AFM probe is heated at a slow, controlled rate of  $0.6 \text{ K}\cdot\text{min}^{-1}$ , the local temperature of the coating in contact with the tip increases. When heated above a certain temperature, the material starts to soften and the tip of the probe is pushed gradually into the coating. This so-called softening temperature  $T_{soft}$  can be determined as the onset point for the tip penetration into the coating material. These temperatures correspond well with the gel transition temperatures simulated using the actual temperature programmes of the LTA probe (conversion rates were calculated using Equation (A3) in Appendix A). For the DPBM-F4000 coating, having the lowest furan and maleimide concentration, the softening temperature is much lower than the simulated gel transition temperature. This could be explained by the low cross-link density and softness of the coating, showing insufficient resistance against the force exerted by the LTA probe tip, even at temperatures well below the gel transition, causing penetration of the probe into the soft coating material to start before the network is dissociated.

The judicious combination of multi-functional building blocks allows tuning of the mechanical properties and the thermal response of the thermoreversible networks. Figure 4 compares the thermomechanical behaviour of the thermoreversible polymer network systems with different cross-link densities. The results are summarized in Table 1. As the average furan-equivalent weight of the furan-containing Jeffamines decreases due to shorter spacer lengths, the concentration of the

active groups, and the resulting crosslink density of the formed network increases. Using this strategy, polymer networks with distinctly different thermomechanical behaviour are obtained, with glass transitions ranging from below  $-50\text{ }^{\circ}\text{C}$  to above  $80\text{ }^{\circ}\text{C}$ . DPBM-F230 and -F400 are hard thermosets with  $T_g$ 's above  $80\text{ }^{\circ}\text{C}$  and storage moduli in the GPa range at  $25\text{ }^{\circ}\text{C}$ , while DPBM-F2000 and DPBM-F4000 are soft elastomers with  $T_g$ 's well below ambient temperature and storage moduli of the order of 10 to 100 MPa.

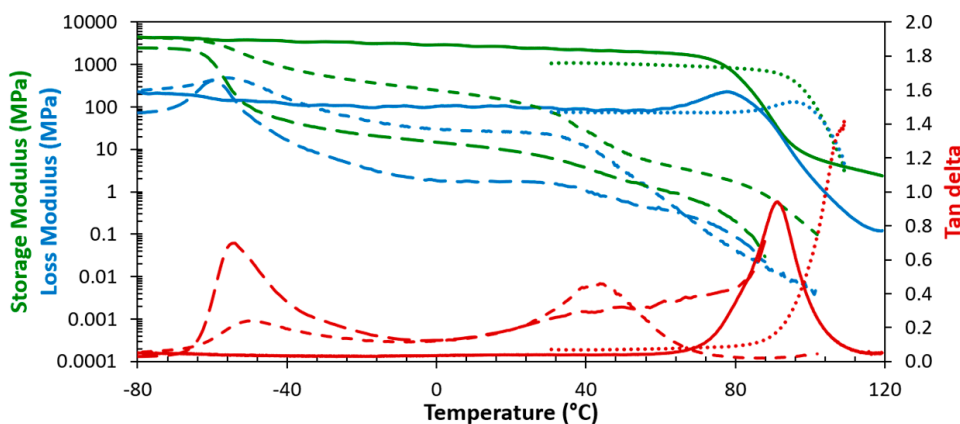


**Figure 4.** Dynamic mechanical analysis (DMA) results comparing the thermomechanical properties of thermoreversible polymer networks with different crosslink densities: DPBM-F230 (dotted), -F400 (solid), -F2000 (short dashed), and -F4000 (long dashed), performed at 0.1% strain and 1 Hz.

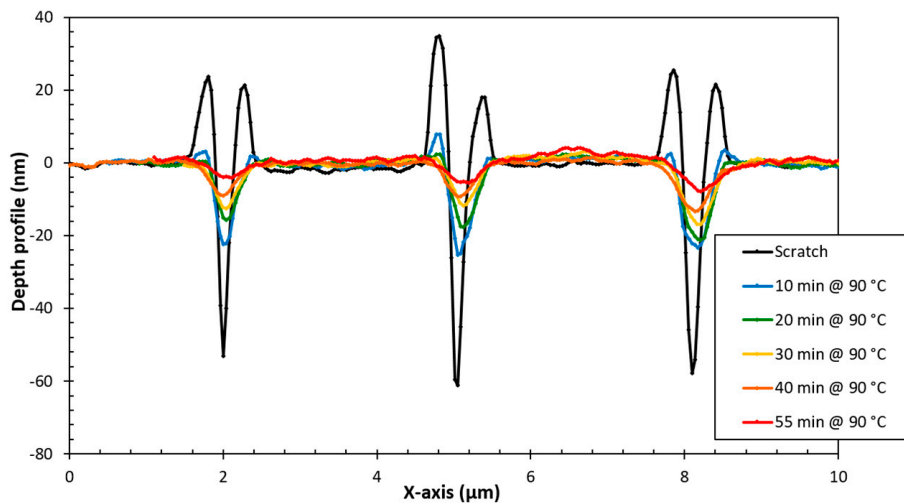
These reversible polymer networks were coated onto aluminium substrates to study their healing behaviour on the microscopic scale and to relate the observed healing to their thermomechanical behaviour.

### 3.2. Dynamically Reversible Polymer Network Coatings

The damage creation and subsequent damage healing of two self-healing coating systems with distinctly different thermomechanical properties are examined and compared. First, microscopic scratches are made in a thermoset coating with a high glass transition temperature and elastic modulus. The scratches are healed at temperatures inside the glass transition region and above. Second, an elastomer coating with a very low glass transition temperature and low modulus is damaged and healed. The healing rate and efficiency are related to their respective thermomechanical properties.

#### 3.2.1. Thermally Reversible Thermoset Coatings

First, the microscopic healing behaviour of the DPBM-F400 is evaluated and applied as a coating onto an aluminium substrate. The coating material is a thermoset at room temperature with a glass transition  $T_g$  of about  $80\text{ }^{\circ}\text{C}$  and an elastic modulus in the GPa range. The nano-lithography option of the AFM was used to create microscopic damages to the coating surface. Using nano-lithography, well-defined forces can be exerted with the AFM tip onto the sample surface, resulting in scratches with well-controlled and reproducible depth and geometry. The evolution of the depth of the scratches in a fixed location is shown in Figure 5 (topography images see Appendix A Figure A1), as the sample is intermittently heated to the isothermal healing temperature for a fixed amount of time and cooled back to room temperature for topography acquisition. The depth of the scratches is shown as a function of the healing times at  $90\text{ }^{\circ}\text{C}$ , showing successful closing of the defects within the time span of 1 h.



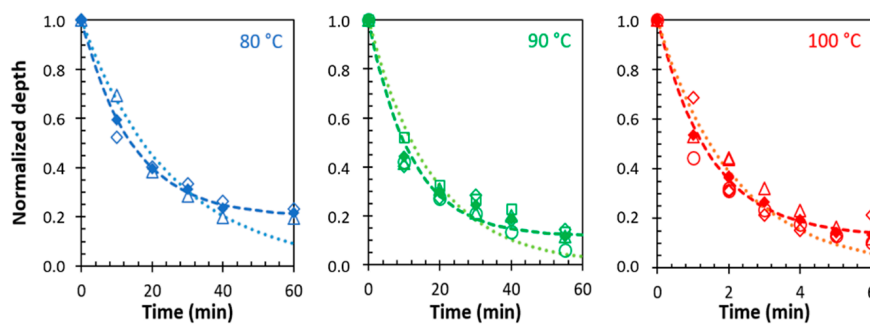
**Figure 5.** Depth profiles of scratches in a DPBM-F400 coating (topography images in Appendix A in Figure A1) as a function of healing time at 90 °C (measured at 40 °C): Fresh scratch (black), healed for 10 min (blue), 20 min (green), 30 min (yellow), 40 min (orange), and 55 min (red).

Figure 6 shows the evolution of the scratch sealing process for healing experiments performed at different temperatures. The depths at multiple locations in different scratches are compared by normalizing the measured depth with respect to the original depth of the scratch. Figure 6 compares the normalized depths as a function of the healing time at different temperatures. The evolution of the (normalized) depths of the scratches was first fitted with an exponential decay, described by Equation (2) and illustrated by the dotted lines in Figure 6. The time constant for the sealing action  $\tau_{\text{seal}}$  was optimized for each temperature individually. The optimized model parameters result in a decent fit at the start of the experiment, but fail to describe the later stages of the sealing event, where experimentally residual damage seems to remain. An improved model, described by Equation (3), takes into account the residual damage  $d_{\infty}$ , and describes the evolution of the depth of the scratches better for all times and temperatures, as shown by the dashed lines in Figure 6.

$$d = d_0 e^{-\frac{t}{\tau_{\text{seal}}}} \tag{2}$$

$$d = d_{\infty} + (d_0 - d_{\infty}) e^{-\frac{t}{\tau_{\text{seal}}}} \tag{3}$$

$$\eta_{\text{seal}} = 1 - \frac{d}{d_0} = 1 - \frac{d_{\infty}}{d_0} - \left(1 - \frac{d_{\infty}}{d_0}\right) e^{-\frac{t}{\tau_{\text{seal}}}} = \eta_{\infty} (1 - e^{-\frac{t}{\tau_{\text{seal}}}}) \tag{4}$$



**Figure 6.** Normalized depths of scratches in a DPBM-F400 coating (empty markers for different experiments). The evolution of the average normalized depth (full markers) is fitted with an exponential decay, as described by Equation (2) (dotted lines) and an exponential decay taking into account residual damage, as described by Equation (3) (dashed lines). Sealing efficiencies in Appendix A Figure A2.

The sealing efficiency  $\eta_{\text{seal}}$  is calculated by Equation (4), with  $\eta_{\infty}$  the maximum healing efficiency for an infinite time, corresponding to the residual damage. The optimized parameters for the improved model (Equation (3)) are listed in Table 2. The time constants quickly decrease with increasing temperature, and the residual damage also decreases with temperature, implying a faster and more efficient sealing. As the healing temperature increases, more reversible crosslinks are broken and the dynamic equilibrium between bond formation and breaking speeds up, resulting in a higher segmental mobility inside the coating material, allowing faster and more efficient sealing of the damage.

**Table 2.** Sealing evaluation using an exponential decay model (basic) and one accounting for residual damage (improved).

DPBM-F400	Model	Temperature	$\tau_{\text{seal}}$ (min)	$\eta_{\infty}$	DPBM-F4000	Model	Temperature	$\tau_{\text{seal}}$ (min)	$\eta_{\infty}$
scratches	improved	80 °C	14.3	80.0%	scratches	improved	70 °C	24.4	37%
		90 °C	12.0	88.4%			75 °C	10.1	71%
		100 °C	1.5	87.1%			80 °C	5.2	82%

It is important to note that the healing of microscopic defects in the DPBM-F400 coatings is feasible below the equilibrium gel point temperature of the bulk material ( $T_{\text{gel,eq}} = 120$  °C) and the corresponding softening temperature ( $T_{\text{soft}} = 114$  °C), observed for the studied coating using local thermal analysis (Figure 3). It can be concluded that enough mobility is created at these healing temperatures to seal the damage, without the need to completely break down the polymer network structure, retaining the mechanical integrity of the coating.

### 3.2.2. Thermally Reversible Elastomeric Coatings

Similar evaluations of the ability to heal microscopic damage were performed for elastomeric DPBM-F4000 coatings with a  $T_g$  of  $-60$  °C. Elastomeric materials are considerably more difficult to damage in a controlled fashion using the nano-lithography option of the AFM. Topography images for line damages in a DPBM-F4000 coating are available in Appendix A (Figure A3). The AFM probe tip experiences less resistance from the elastomeric material, allowing the probe to sink deeper into the coating surface. When trying to scratch the surface along a line path, the probe tip jumps out of and back into contact with the scratched surface due to the elasticity of the coating material, creating  $\mu\text{m}$  sized defects and moving large amounts of debris along the path of the scratch, making it impossible to perform a truly quantitative analysis of the topography and depths of the created defects. Nevertheless, the sealing capabilities of these thermally reversible networks are clear from the topography evolution as a function of time at temperatures ranging from 70 to 85 °C, as shown in Figure 7. Due to the removal of material from the damage area by the AFM tip, there can be a considerable amount of residual damage, implying that the model that takes into account residual damage is most suited to describe the damage sealing event. Table 2 shows how the sealing rates and efficiencies increase with increasing temperature and resulting mobility. Similar to the DPBM-F400 thermoset coating, all healing temperatures are below the equilibrium gel point temperature of the bulk material ( $T_{\text{gel,eq}} = 91$  °C) and the softening temperature ( $T_{\text{soft}} = 85$  °C) observed for the studied coating (Figure 3).

### 3.3. Temperature Dependence of the Sealing Mechanism

The previous sections illustrated how the sealing of the microscopic damage becomes faster and more efficient with increasing temperature for the DPBM-F400 thermoset coating (Section 3.2.1) and for the DPBM-F4000 elastomer coating (Section 3.2.2). For the latter coating system, a linear relationship is found between the natural logarithm of the sealing time constant  $\tau_{\text{seal}}$  and the reciprocal sealing temperature, with an activation energy of  $123 \text{ kJ}\cdot\text{mol}^{-1}$ , as shown in the Arrhenius plot in Figure 8 (rhombi). Shorter sealing times at higher temperatures confirm faster sealing of the microscopic damage.

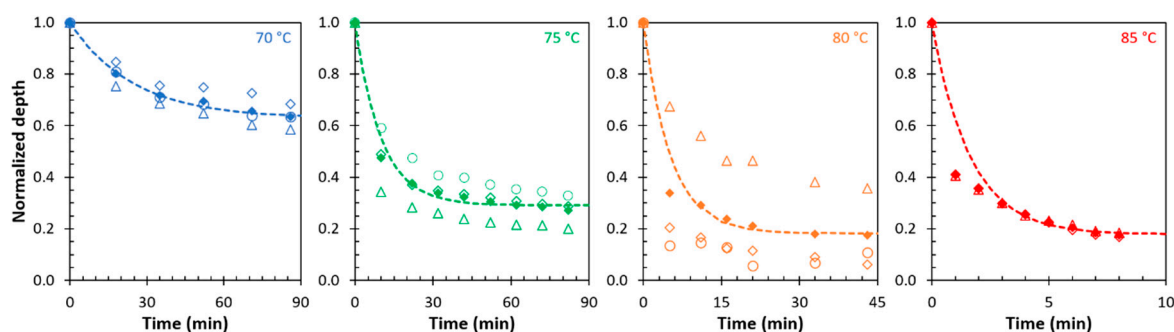


**Figure 7.** Normalized depths of scratches in a DPBM-F4000 coating (empty markers for different experiments) as a function of healing time at different temperatures. The evolution of the average normalized depth (full markers) is fitted to an exponential decay taking into account residual damage (dashed lines, Equation (3)). Sealing efficiencies in Appendix A (Figure A4).

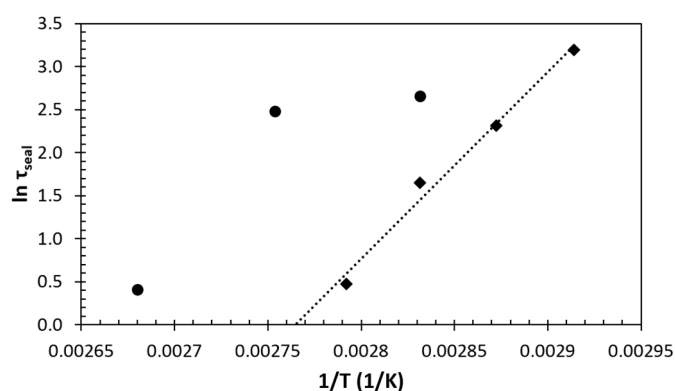


**Figure 8.** Natural logarithm of the sealing time constants for the heating-mediated sealing of microscopic damage for the DPBM-F400 (circles) and DPBM-F4000 (rhombi) thermoreversible polymer network coatings.

Higher temperatures are required to seal microscopic damage in the more densely crosslinked DPBM-F400 thermoset coating (circles) than in the elastomer coating. The two highest sealing temperatures (90 and 100 °C) for the thermoset coating show a similar slope and activation energy as the elastomer coating, while  $\tau_{\text{seal}}$  deviates strongly from this slope at the lowest studied temperature (80 °C). This temperature is nearly equal to the  $T_g$  of the network (79 °C), which possibly results in partial vitrification slowing down the reaction kinetics and strongly influencing the mechanical properties and related sealing behaviour. In the next section, the temperature dependence of the sealing event will be confronted with the thermomechanical behavior of the bulk materials (studied in Section 3.1.1).

### 3.4. Structure-Property Relation of the Sealing Mechanism

It should be noted that the concentration of the reactive groups has an impact on the reaction kinetics and the equilibrium conversion, influencing the healing kinetics. Furthermore, the concentration and conversion of the Diels-Alder groups directly affects the crosslink density of the polymer network, which in turn defines the mechanical properties, as illustrated in Figure 4 in Section 3.1.1. The rubber elasticity theory relates the shear modulus of an ideal rubber to the concentration of effective network chains  $\nu$  that serve as entropic springs, the ideal gas constant  $R$  and temperature  $T$  (Equation (5)).

$$G = \nu RT = (\nu_c + \nu_e)RT \quad (5)$$

Network chains formed by chemical crosslinks  $\nu_c$  and entanglements  $\nu_e$  both contribute to the elastic behavior [29]. The theory assumes that the effective network chains are long enough

so they can assume a random coil conformation and end at effective crosslinking points. Since the rubber elastic theory applies most accurately to elastomeric materials with sufficiently low crosslink density, at temperatures well above their  $T_g$ , the most elastic DPBM-F4000 coating will be considered. In case of the thermally reversible polymer networks, where the Diels-Alder adducts serve as reversible crosslinks, the number of formed crosslinks depends on the reaction conversion and thus on temperature and time. The remainder of unreacted furan and maleimide groups results in dangling chain ends, of which the amount consequently also depends on conversion. Hence,  $\nu_c$  and  $\nu_e$  in Equation (5) depend on temperature and time, in contrast to traditional irreversibly crosslinked polymer networks where both values are constant after the crosslinking reaction has completed. Figure 9 shows the conversion as a function of time for the quasi-isothermal temperature profiles used to seal the damage at different temperatures. With increasing time at the elevated temperatures, the conversion continues to decrease until it nears the equilibrium conversion at that temperature.

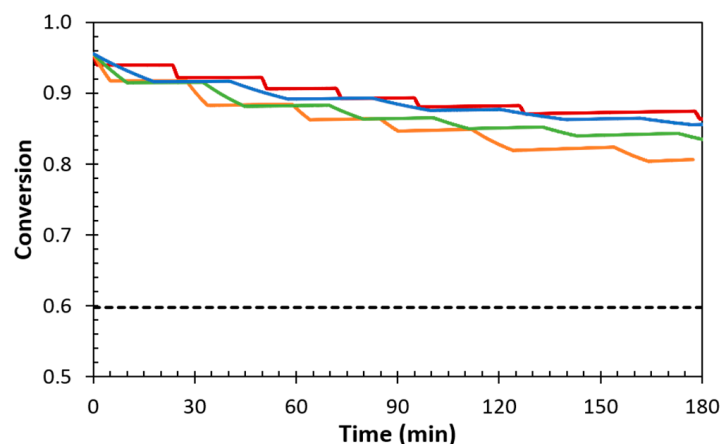


**Figure 9.** Conversion profiles for the quasi-isothermal heat treatments of the DPBM-F4000 coating at 70 °C (blue), 75 °C (green), 80 °C (orange), and 85 °C (red), as compared to the critical gel point conversion (dashed line). Temperature profiles are given in Figure A5.

As adduct bonds are broken, the number of crosslinks in the network decreases and the number of dangling chains increases, both adding to the mobility of the polymer chains responsible for sealing the damage. In general, the viscoelastic behaviour of the polymer network is described by the complex modulus  $E^*$ , which is a combination of the storage modulus  $E'$  (real component) quantifying the elastic contribution of the network chains, and the loss modulus  $E''$  (imaginary component) quantifying the viscous contribution (see also Figure 4). It is safe to assume that both the decrease in the number of network chains, the resulting increase in flexibility and thus decreasing  $E'$ , and the increase in the number of dangling chains and overall decreasing  $E''$  will contribute to the sealing efficiency. The complex modulus  $E^*$  represents the resistance of the viscoelastic material against deformation. Consequently, this decrease in resistance against deformation results in faster and more efficient healing, as shown by plotting the natural logarithm of the sealing time constants  $\tau_{\text{seal}}$  against the natural logarithm of the complex modulus  $E^*$  (Figure 10). A linear trend is observed for the elastomeric coating (rhombi), corresponding to a power law relationship between  $\tau_{\text{seal}}$  and  $E^*$ . The thermoset coating (circles) follows a similar trend for the highest temperatures (lowest  $E^*$  values), while  $\tau_{\text{seal}}$  at the lowest temperature or highest  $E^*$  value seems to level off as the material goes into its glass transition. In the glass transition region the segmental mobility of the polymer chains starts to be restricted, thus slowing down the reaction kinetics and reducing the sealing ability of the coating. Still, successful sealing of the incurred damage was demonstrated at 80 °C in times comparable to the sealing at 90 °C, at the end of the glass transition, only to speed up further at higher temperatures (Figure 8).

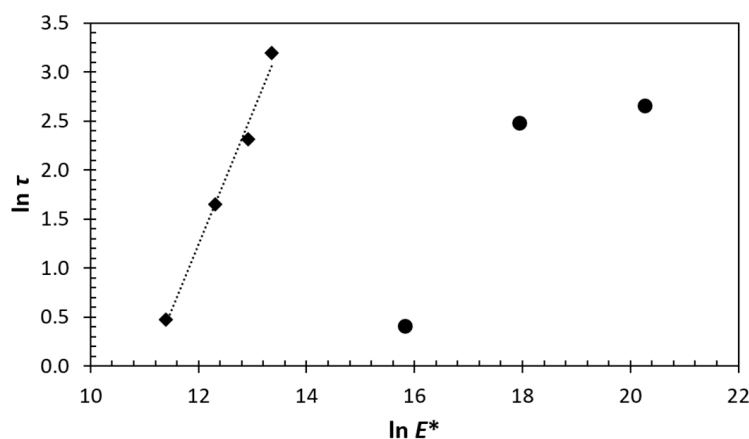


**Figure 10.** Natural logarithm of the sealing time constants as a function of the natural logarithm of the complex modulus for the heating-mediated sealing of microscopic damage for the DPBM-F400 (circles) and DPBM-F4000 (rhombi) thermoreversible polymer network coatings.

#### 4. Discussion

The thermoreversible behaviour of a series of coatings, crosslinked through the reversible Diels-Alder reaction, were compared to the thermomechanical properties of the bulk material. Coatings with glass transition temperatures ranging from  $-60\text{ }^{\circ}\text{C}$  to  $95\text{ }^{\circ}\text{C}$  were prepared. A good agreement was found between the experimental equilibrium gel point temperatures of the bulk materials, the softening temperatures of the coatings, and the simulated gel point temperatures.

Microscopic damage was applied by nano-lithography to a DPBM-F400 coating with a high crosslink density ( $T_g$  of  $79\text{ }^{\circ}\text{C}$ ), and an elastomeric DPBM-F4000 coating with a low crosslink density ( $T_g$  of  $-60\text{ }^{\circ}\text{C}$ ). For both coating systems, the sealing of the damage was followed quasi-isothermally using Atomic Force Microscopy at temperatures between their  $T_g$  and  $T_{gel}$ , to ensure sufficient mobility to seal damage, while retaining enough mechanical integrity. The variation of the sealing efficiency with time was fitted to an empirical model that describes the reduction of damage as a function of time by means of a sealing time constant, taking into account residual damage.

A faster and more effective sealing (less residual damage) is observed at higher temperatures. The time constants for the sealing of damage in the elastomer network could be described by an Arrhenius law. A clear trend was found between the sealing time constants of this elastomer coating at different temperatures and the corresponding complex moduli, describing the resistance against deformation of the viscoelastic material at that temperature. For the thermoset coating, vitrification and diffusion control of reaction rates seem to influence the sealing ability of the coating at temperatures close to  $T_g$ . For this more densely crosslinked coating, higher sealing temperatures are required to obtain the necessary mobility to achieve successful damage sealing at a rate comparable to the elastomer coating (similar sealing time constant). Notwithstanding this, the thermoset coating showed successful damage sealing, even at temperatures inside the glass transition region. However, no clear relationship between the sealing time constants and the complex moduli was found, possibly due to the added complexity of the mechanical behaviour close to the glass transition.

The good agreement between the local thermal analysis (LTA) techniques and bulk thermal analysis techniques confirms that LTA can be used to study the reversible gel transition of dynamic covalent networks, such as the studied coatings based on the furan-maleimide Diels-Alder chemistry. The combined use of nano-indentation to create microscopic damage, atomic force microscopy (AFM) for topography imaging, and the information from LTA measurements provides excellent tools to study the sealing event of controlled damage in a coating. The addition of a local mechanical evaluation during healing would provide the last tool that would complete the study, as it also allows to follow the recovery of the mechanical properties of the coating and related barrier properties.

**Author Contributions:** Conceptualization, J.B.; Methodology, J.B.; Software, R.V.; Validation J.B., R.V. and J.M.; Formal Analysis, J.B.; Investigation, Jessica Mangialetto; Resources, G.V.A.; Data Curation, J.B.; Writing—Original Draft Preparation, J.B.; Writing—Review and Editing, G.V.A.; Visualization, J.B.; Supervision, G.V.A.; Project Administration, G.V.A.; Funding Acquisition, G.V.A.

**Funding:** The research was funded by the FONDS WETENSCHAPPELIJK ONDERZOEK (FWO) (No. 12W4719N).

**Acknowledgments:** Huntsman Corporation is thanked for supplying the Jeffamine D series amine hardeners.

**Conflicts of Interest:** The authors declare no conflict of interest.

## Appendix A

**Table A1.** Kinetic parameters for the Diels-Alder reaction between DPBM and FXXX.

Kinetic Parameter	Endo Isomer	Exo Isomer
$\ln A_{DA}$ ( $\text{kg}\cdot\text{mol}^{-1}\cdot\text{s}^{-1}$ )	15.8	16.4
$E_{DA}$ ( $\text{kJ}\cdot\text{mol}^{-1}$ )	65.1	73.7
$\ln A_{rDA}$ ( $\text{s}^{-1}$ )	27.9	37.1
$E_{rDA}$ ( $\text{kJ}\cdot\text{mol}^{-1}$ )	101.3	137.1
$\Delta_r H^\circ$ ( $\text{kJ}\cdot\text{mol}^{-1}$ )	-36.2	-63.4
$\Delta_r S^\circ$ ( $\text{kJ}\cdot\text{mol}^{-1}\cdot\text{K}^{-1}$ )	-100.5	-172.3

$$k_i = A_i e^{-\frac{E_i}{RT}} \quad (\text{A1})$$

$$K = K_{\text{endo}} + K_{\text{exo}} = \frac{k_{DA,\text{endo}}}{k_{rDA,\text{endo}}} + \frac{k_{DA,\text{exo}}}{k_{rDA,\text{exo}}} \quad (\text{A2})$$

$$\frac{dx}{dt} = k_{DA,\text{endo}}[F][M] - k_{rDA,\text{endo}}[A_{\text{endo}}] + k_{DA,\text{exo}}[F][M] - k_{rDA,\text{exo}}[A_{\text{exo}}] \quad (\text{A3})$$

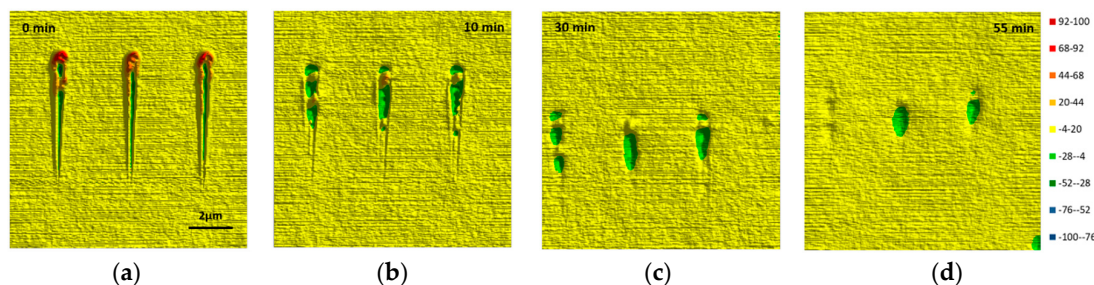


**Figure A1.** Topography images of a DPBM-F400 coating, scratched by nano-lithography and healed at 90 °C for increasing isothermal times, using an in-situ heating stage in the AFM: (a) 0 min; (b) 10 min; (c) 30 min; (d) 55 min.

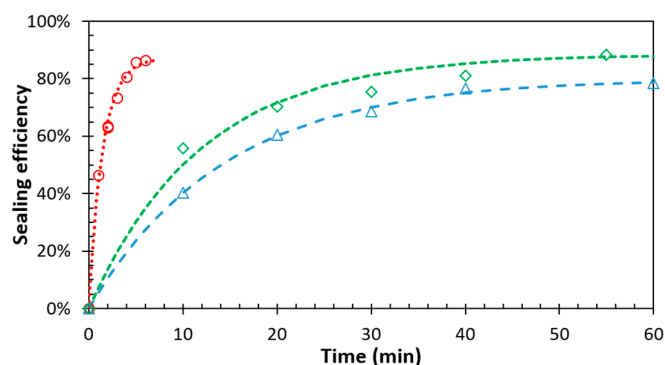


**Figure A2.** Sealing efficiency, based on the depths of the scratches shown in Figure 5, for the average of a series of scratches (symbols) and the optimized fit using Equation (3) (lines) as a function of time at 80, 90 and 100 °C.

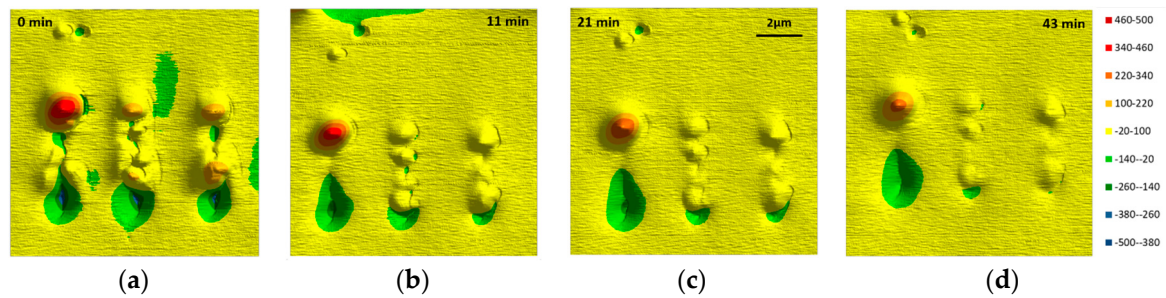


**Figure A3.** Topography images of a DPBM-F4000 coating, scratched by nano-lithography and healed at 90 °C for increasing isothermal times, using an in-situ heating stage in the AFM: (a) 0 min; (b) 11 min; (c) 21 min; (d) 43 min.

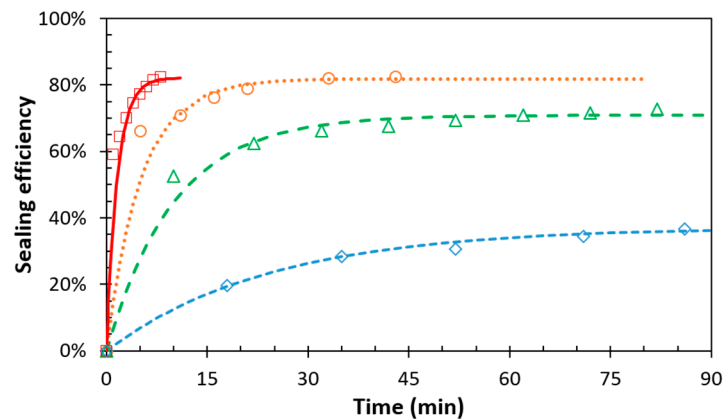


**Figure A4.** Sealing efficiency of the DPBM-F4000 coating for the average of a series of scratches (symbols) and the optimized fit (lines) as a function of time at 70, 75, 80 and 85 °C.

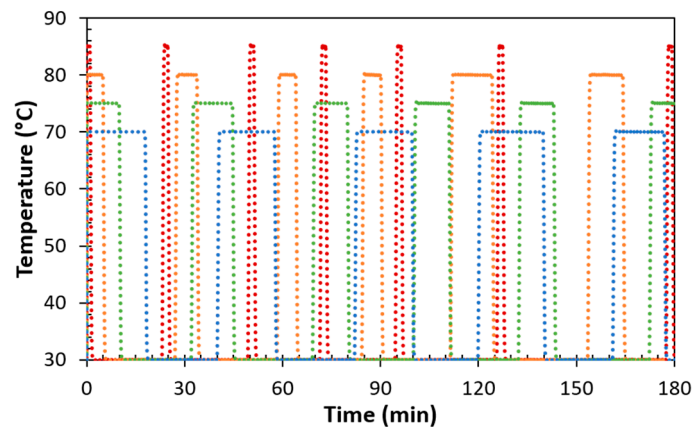


**Figure A5.** Temperature profiles for the sealing of microscopic damage of the DPBM-F4000 coating during quasi-isothermal experiments at 70 (blue), 75 (green), 80 (orange) and 85 °C (red).

## References

1. Esteves, C. Self-healing functional surfaces. *Adv. Mater. Interfaces* **2018**, *5*, 1800293. [[CrossRef](#)]
2. Shchukin, D.G.; Möhwald, H. Self-repairing coatings containing active nanoreservoirs. *Small* **2007**, *3*, 926–943. [[CrossRef](#)] [[PubMed](#)]
3. Cho, S.H.; White, S.R.; Braun, P.V. Self-healing polymer coatings. *Adv. Mater.* **2009**, *21*, 645–649. [[CrossRef](#)]
4. Samadzadeh, M.; Boura, S.H.; Peikari, M.; Kasiriha, S.M.; Ashrafi, A. A review on self-healing coatings based on micro/nanocapsules. *Prog. Org. Coat.* **2010**, *68*, 159–164. [[CrossRef](#)]

5. Toohey, K.S.; Sottos, N.R.; Lewis, J.A.; Moore, J.S.; White, S.R. Self-healing materials with microvascular networks. *Nat. Mater.* **2007**, *6*, 581–585. [[CrossRef](#)] [[PubMed](#)]
6. Torre-Muruzabal, A.; Daelemans, L.; van Assche, G.; de Clerck, K.; Rahier, H. Creation of a nanovascular network by electrospun sacrificial nanofibers for self-healing applications and its effect on the flexural properties of the bulk material. *Polym. Test.* **2016**, *54*, 78–83. [[CrossRef](#)]
7. Wietor, J.L.; Dimopoulos, A.; Govaert, L.E.; van Benthem, R.A.T.M.; de With, G.; Sijbesma, R.P. Preemptive healing through supramolecular cross-links. *Macromolecules* **2009**, *42*, 6640–6646. [[CrossRef](#)]
8. Li, Y.; Fang, X.; Wang, Y.; Ma, B.; Sun, J. Highly transparent and water-enabled healable antifogging and frost-resisting films based on poly(vinyl alcohol)-Nafion complexes. *Chem. Mater.* **2016**, *28*, 6975–6984. [[CrossRef](#)]
9. Wouters, M.; Craenmehr, E.; Tempelaars, K.; Fischer, H.; Stroeks, N.; van Zanten, J. Preparation and properties of a novel remendable coating concept. *Prog. Org. Coat.* **2009**, *64*, 156–162. [[CrossRef](#)]
10. Scheltjens, G.; Brancart, J.; de Graeve, I.; van Mele, B.; Terry, H.; van Assche, G. Self-healing property characterization of reversible thermoset coatings. *J. Therm. Anal. Calorim.* **2011**, *105*, 805–809. [[CrossRef](#)]
11. Imbesi, P.M.; Fidge, C.; Raymond, J.E.; Cauët, S.I.; Wooley, K.L. Model Diels-Alder studies for the creation of amphiphilic cross-linked networks as healable, antibiofouling coatings. *ACS Macro Lett.* **2012**, *1*, 473–477. [[CrossRef](#)]
12. Kötteritzsch, J.; Stumpf, S.; Hoepfner, S.; Vitz, J.; Hager, M.D.; Schubert, U.S. One-component intrinsic self-healing polymer for coatings based on reversible crosslinking by Diels-Alder-cycloaddition, *macromol. Chem. Phys.* **2013**, *214*, 1636–1649.
13. Barthel, M.J.; Rudolph, T.; Teichler, A.; Paulus, R.M.; Vitz, J.; Hoepfner, S.; Hager, M.D.; Schacher, F.H.; Schubert, U.S. Self-healing materials via reversible crosslinking of poly(ethylene oxide)-block-poly(furfuryl glycidyl ether) (PEO-b-PFGE) block copolymer films. *Adv. Funct. Mater.* **2013**, *23*, 4921–4932. [[CrossRef](#)]
14. Turkenburg, D.H.; Durant, Y.; Fischer, H.R. Bio-based self-healing coatings based on thermo-reversible Diels-Alder reaction. *Prog. Org. Coat.* **2017**, *111*, 38–46. [[CrossRef](#)]
15. Zheludkevich, M.L.; Tedim, J.; Ferreira, M.G.S. “Smart” coatings for active corrosion protection based on multi-functional micro and nanocontainers. *Electrochim. Acta* **2012**, *82*, 314–323. [[CrossRef](#)]
16. Lutz, A.; van den Berg, O.; Wielant, J.; de Graeve, I.; Terry, H. A Multiple-action self-healing coating. *Front. Mater.* **2016**, *2*, 73. [[CrossRef](#)]
17. Andreeva, D.V.; Shchukin, D.G. Smart self-repairing protective coatings. *Mater. Today* **2008**, *11*, 24–30. [[CrossRef](#)]
18. Chuo, T.W.; Liu, Y.L. Furan-functionalized aniline trimer based self-healing polymers exhibiting high efficiency of anticorrosion. *Polymer* **2017**, *125*, 227–233. [[CrossRef](#)]
19. Diaz, M.M.; Brancart, J.; van Assche, G.; van Mele, B. Room-temperature versus heating-mediated healing of a Diels-Alder crosslinked polymer network. *Polymer* **2018**, *153*, 453–463. [[CrossRef](#)]
20. Brancart, J.; Scheltjens, G.; Muselle, T.; van Mele, B.; Terry, H.; van Assche, G. Atomic force microscopy-based study of self-healing coatings based on reversible polymer network systems. *J. Intell. Mater. Syst. Struct.* **2014**, *25*, 40–46. [[CrossRef](#)]
21. Yoon, J.A.; Kamada, J.; Koynov, K.; Mohin, J.; Nicola, R.; Zhang, Y.; Balazs, A.C.; Kowalewski, T.; Matyjaszewski, K. Self-healing polymer films based on thiol-disulfide exchange reactions and self-healing kinetics measured using atomic force microscopy. *Macromolecules* **2012**, *45*, 142–149. [[CrossRef](#)]
22. Kim, S.Y.; Lee, T.H.; Park, Y.I.; Nam, J.H.; Noh, S.M.; Cheong, I.W.; Kim, J.C. Influence of material properties on scratch-healing performance of polyacrylate-graft-polyurethane network that undergo thermally reversible crosslinking. *Polymer* **2017**, *128*, 135–146. [[CrossRef](#)]
23. González-García, Y.; Santana, J.J.; González-Guzmán, J.; Izquierdo, J.; González, S.; Souto, R.M. Scanning electrochemical microscopy for the investigation of localized degradation processes in coated metals. *Prog. Org. Coat.* **2010**, *69*, 110–117. [[CrossRef](#)]
24. González, S.; Santana, J.J.; González-García, Y.; Fernández-Mérida, L.; Souto, R.M. Scanning electrochemical microscopy for the investigation of localized degradation processes in coated metals: Effect of oxygen. *Corros. Sci.* **2011**, *53*, 1910–1915. [[CrossRef](#)]
25. Scheltjens, G.; Diaz, M.M.; Brancart, J.; van Assche, G.; van Mele, B. A self-healing polymer network based on reversible covalent bonding. *React. Funct. Polym.* **2013**, *73*, 413–420. [[CrossRef](#)]

26. Diaz, M.M.; van Assche, G.; Maurer, F.H.J.; van Mele, B. Thermophysical characterization of a reversible dynamic polymer network based on kinetics and equilibrium of an amorphous furan-maleimide Diels-Alder cycloaddition. *Polymer* **2017**, *120*, 176–188. [[CrossRef](#)]
27. Cuvellier, A.; Verhelle, R.; Brancart, J.; Vanderborght, B.; van Assche, G.; Rahier, H. The influence of stereochemistry on the reactivity of the Diels-Alder cycloaddition and the implications for reversible network polymerization. *Polym. Chem.* **2019**, in press. [[CrossRef](#)]
28. Winter, H.; Chambon, F. Analysis of linear viscoelasticity of a crosslinking polymer at the gel point. *J. Rheol.* **1986**, *30*, 367–382. [[CrossRef](#)]
29. Miller, D.R.; Macosko, C.W. A New derivation of post gel properties of network polymers. *Macromolecules* **1976**, *9*, 206–211. [[CrossRef](#)]



© 2018 by the authors. Licensee MDPI, Basel, Switzerland. This article is an open access article distributed under the terms and conditions of the Creative Commons Attribution (CC BY) license (<http://creativecommons.org/licenses/by/4.0/>).